cambridge.org/jog

Tracking glacier surge evolution using interferometric SAR coherence—examples from Svalbard

Erik Schytt Mannerfelt[1,2] [ID], Thomas Schellenberger[1] [ID] and Andreas M. Kääb[1] [ID]

[1]Department of Geosciences, University of Oslo, Oslo, Norway and [2]Arctic Geology, The University Centre in Svalbard, Longyearbyen, Norway

Abstract

We present a practically simple methodology for tracking glacier surge onset and evolution using interferometric synthetic aperture radar (InSAR) coherence. Detecting surges early and monitoring their build-up is interesting for a multitude of scientific and safety-related aspects. We show that InSAR coherence maps allow the detection of surge-related instability on Svalbard many years before being detectable by, for instance, feature tracking or crevasse detection. Furthermore, we present derived data for two types of surges; down- and up-glacier propagating, with interestingly consistent surge propagation and post-surge relaxation rates. The method works well on Svalbard glaciers, and the data and core principle suggest a global applicability.

1. Introduction

Glacier surges are sudden temporary glacier speed-ups, sometimes by one or several orders of magnitudes. Related factors such as substantial mass transfer, change in surface morphology and the timescale of months to decades are also often included in the definition. The occurrence of this behaviour is concentrated in clusters globally (Sevestre and Benn, 2015; Kääb and others, 2023) with Svalbard being one of these significant clusters. Surges pose local safety hazards by damming lakes that subsequently outburst (Post and Mayo, 1971; Bazai and others, 2021), or for travel across glaciers, and reveal problems in our understanding of general glacier dynamics due to our inability to properly predict them. In situ studies of glaciers on the brink of surging yield invaluable information (e.g. Clarke, 1976; Bouchayer and others, 2024), but the lack of indications before surges means they are generally not known before it is too late to study their evolution in entirety. Here, we present a new method for detecting glacier surges years before they become detectable by established methods and demonstrate it on glaciers on Svalbard, presenting statistics on the rates of surge evolution throughout the archipelago.

Previous methods of surge detection involve identifying sudden changes in geometry, texture or surface velocity of a glacier, and we summarise selected studies in the following overview. We focus our background contextualisation on detection methods over mechanisms; for an in-depth review on Svalbard surges, we refer the reader to Harcourt and others 2025. Elevation change maps reveal large mass displacement events that can be associated with surge-like instabilities (e.g. Sund and others, 2009; Paul and others, 2022). If the surface velocity is high enough, i.e. when a surge has accelerated sufficiently, it can be autonomously detected using feature tracking (surface velocity) time series (e.g. Bhambri and others, 2017; Koch and others, 2023). Unstable flow such as surging can also be detected by geometrical changes in medial moraines (Herreid and Truffer, 2016). The detection of drastic increases in crevassing is finally a robust method of identifying an ongoing surge through subtracting synthetic aperture radar (SAR) backscatter intensity images over time (Kääb and others, 2023). While all of these methods work well on their own, they mostly function when the glacier is either fully surging or has already terminated; characterising the build-up is much more difficult. High-accuracy elevation data can technically be used over long time periods to reveal unstable mass redistribution associated with future surging (Sund and others, 2009). Acquiring these elevation data at high accuracy and temporal frequency requires thorough processing and error assessment, however (cf. Hugonnet and others, 2022), and finding an easier and less resource-intensive method would clearly be advantageous.

Repeated SAR acquisitions of terrain can be used to assess changes in signal phase, affected by terrain motion, and changes in reflective characteristics. Interferometric SAR (InSAR), the process of describing these phase changes, is commonly used in cryospheric sciences, e.g. for ground subsidence (Rouyet and others, 2021), glacier velocity (Eldhuset and others, 2003) and classification of debris-covered glaciers (Thomas and others, 2023). While normal InSAR workflows generally involve heavy processing to obtain displacement products, a simpler and useful by-product is the normalised cross-correlation of two single-look complex SAR scenes,
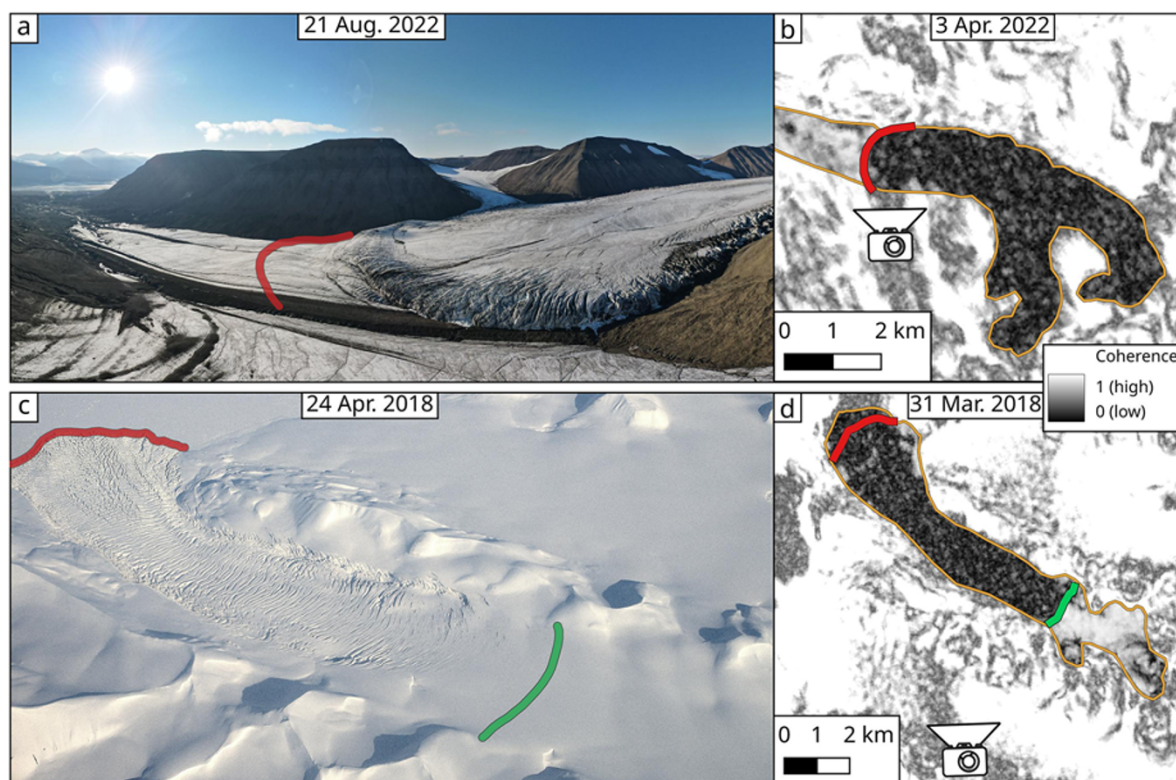
Figure 1. Photographs compared to coherence maps in the same year. (a) Down-glacier propagating surge of Vallåkrabreen, showing a surge bulge with splaying crevasses and a less pronounced forebulge ahead of it (photograph credit: Leonard Magerl). The red line shows the approximate location of the low-coherence boundary from earlier that year (shown in (b)), together with the photo location; roughly coincident with the forebulge. (c) Up-glacier propagating surge of Arnesenbreen (photograph credit: Erik S. Mannerfelt), showing the lower surge boundary in red and the upper low-coherence boundary in green (cf. panel (d)). We presume that the discrepancy between the green line in (c) and the region of substantial crevassing is due to coherence being sensitive to smaller disturbances than what can be seen in a winter photograph. The largest surge extent (so far) is shown in yellow outlines for panels (b) and (d). The dates of the coherence maps represent the latter dates of the acquisition pairs. Areas outside the largest surge extents have reduced contrast to enhance visibility.

usually denoted as coherence. InSAR coherence varies in the range of 0 (no phase correlation between two acquisitions) to 1 (the phase between acquisitions is identical) and is normally used for quality assessment of the co-registration (Eldhuset and others, 2003), masking out low-coherence areas within phase unwrapping, and terrain classification (Shi and others, 2019), including mapping of debris-covered parts of glaciers that are difficult to delineate using optical methods (Atwood and others, 2010; Frey and others, 2012). Coherence is normally lost either if terrain displacement or its gradients (acceleration, shear, rotation, etc.) become too large or if terrain reflective characteristics change, for example during a rainfall event or during ice- or snowmelt (Weydahl, 2001). Thus, in intervals featuring stable cold weather, the presence or absence of significant glacier motion, motion gradients and deformation can be assessed visually or computationally using InSAR coherence maps. For applications of InSAR coherence in glacier surging specifically, it has previously been used for masking or quality assessing InSAR-derived velocity or topographic products (Strozzi and others, 2002), for the indication of slow surface velocities nearing stagnation (Pritchard and others, 2003) and for a general explanation of the loss of data beyond a threshold of velocity (Strozzi and others, 2002; Murray and others, 2003a). In contrast to these previous studies, we consider the loss of coherence as the primary signal in our method, instead of it acting as an explanatory dataset to contextualise where another product fails.

At least a third, and likely much more, of all glaciers on Svalbard have a recent past of surging (Sevestre and Benn, 2015; Farnsworth

and others, 2016), meaning many currently non-surging glaciers can be described as being in quiescence. Quiescent glacier surface velocities are usually low, measuring $5–18\,\mathrm{m\,a^{-1}}$ on Svalbard (Nuttall and others, 1997; Sund and Eiken, 2004; Sund and others, 2014). Surges dramatically elevate this speed to several or tens of metres per day; an order-of-magnitude increase that is well suited for detection. Two types of surge propagation directions have been shown as prevalent on Svalbard; down-glacier propagating, characterised by a surface bulge (e.g. Murray and others, 1998), or up-glacier propagating, i.e. in a terminus initiated surge (Sevestre and others, 2018). In Alaska, synchronous up- and down-glacier propagation of a surge that initiates in the central body has been shown (Altena and others, 2019), a mechanism that seems rare on Svalbard (Monacobreen; Murray and others, 2003b). We, therefore, focus our present method demonstration on one-directional surge propagation, but our approach could be adapted to synchronous up- and down-glacier propagation in the future. Improved monitoring of surge propagation would contribute to better characterising and understanding of the (potentially different) types of surge evolution and its direction with respect to the direction of glacier flow.

We demonstrate the usefulness of InSAR coherence maps on Svalbard for tracking down- or up-glacier propagating surges by mapping out zones of low coherence (disturbed flow) and measuring temporal changes in their extent. Our resultant patterns show that the technique opens new doors to ways of quantifying surging and allows for rough empirical predictions of the timing of surge
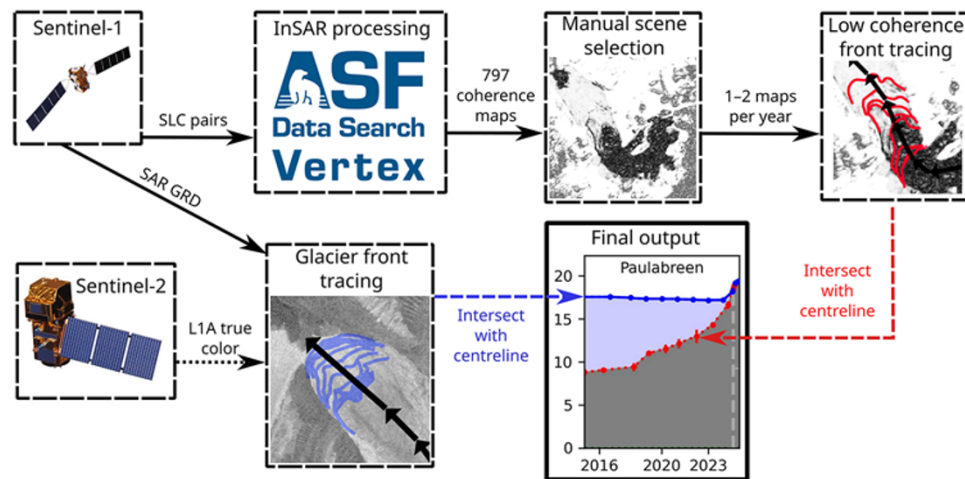
Figure 2. Conceptual diagram of the acquisition and processing of the data. The data examples are from Paulabreen (Figure 4e–h) and showcase the delineation of the lower low-coherence boundary (red) and terminus positions (blue) for its plot in Figure 5e (see that caption for a further explanation of the plot). For up-glacier propagating low-coherence fronts, there is an additional step (green lines, e.g. in Figure 1) to delineate the upper boundary. The latter date in the acquisition pair for the exemplified coherence map ('Manual scene selection' box) is 1 April 2020, and the SAR backscatter image ('Glacier front tracing' box) date is 24 December 2024.
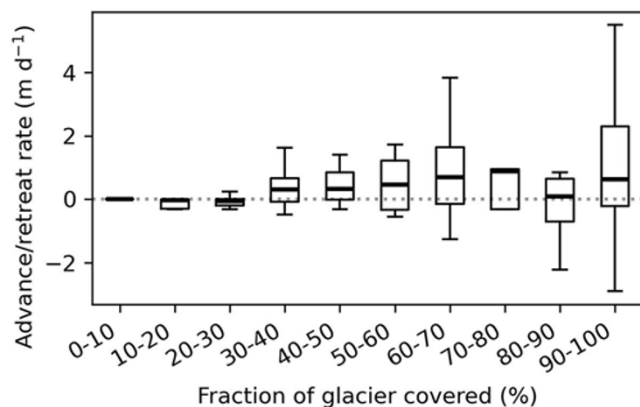

Figure 3. Boxplot comparison of the fraction of low coherence and terminus fluctuation rate at up-glacier propagating (terminus initiated) surges. This was used to derive the 40% threshold as a common starting point for these surges; the 40–50% bin is the first and only bin where the first quartile (the lower box boundary) is above $0\,\mathrm{m\,d^{-1}}$.

acceleration. While our study focuses on Svalbard only, the data and techniques can be used for global assessments of surge propagation rates and patterns in regions with similarly low quiescent baseline flow.

2. Data and methods

We obtain processed Sentinel-1 InSAR coherence maps from the Alaska Satellite Facility (ASF) Vertex tool (https://search.asf.alaska.edu). We order the processing of every 12 day acquisition pair since the beginning of the Sentinel-1 record on Svalbard (January 2015) in the winter months of 1 November to 30 April. We choose this interval as spring or summer melt strongly reduces the phase coherence over entire glaciers and renders the data unusable for our purposes. Qualitative assessments of 6 day returns using the Sentinel-1A and -B satellites revealed much cleaner coherence maps, but we stayed consistent with 12 day baselines as the 6 day availability period lasted only a subset of the study period (October 2016 to December 2021) due to the failure of Sentinel-1B. A total of

797 scenes were successfully processed, with some failures due to co-registration errors not converging below a threshold (defined in the ASF pipeline). Most 12 day pairs show very low coherence throughout the scene due to weather effects (Weydahl, 2001). We sift through the entire catalogue manually for each glacier and extract at least one suitable coherence map per year. For each good scene, we manually delineate any encountered low-coherence front with an upper and/or lower boundary line. A detailed investigation of the influence and the spatio-temporal variations of factors that contribute to coherence loss at the surge fronts (in particular likely motion magnitude, motion gradients, surface deformation and surface changes by crevasse formation) is out of scope for this brief method demonstration. However, comparison of our coherence-derived surge fronts to in situ photographs (Fig. 1) and DEM differences between occasional individual ArcticDEM products shows that our coherence-derived surge fronts coincide with topographic bulges, thus indicating a change in glacier mass transport and dynamics. To obtain terminus positions, we download Sentinel-1 backscatter intensity and Sentinel-2 L1C true colour scenes for manual terminus delineation. We assess length and length change along a manually drawn glacier centreline, measuring the glacier terminus, and the lower and upper low-coherence fronts. We measure lengths of parallel lines within a ±200 m buffer of the centreline to obtain a spread and to reduce uncertainty in the exact placement of the centreline. The chosen buffer width of ±200 m is open to discussion, but not critical for this method demonstration study. The process of our methodology up until this point is summarised in Figure 2.

In order to derive further statistics of the mapped surges, we divide them in three stages (if observed); pre-surge, surge and post-surge, based on our available data. The surge onset date is defined differently for down- and up-glacier propagating surges. For down-glacier propagating surges, we simply assign the latter date of the acquisition pair when the low-coherence front (surge bulge) reaches the terminus. Because of the sparse temporal resolution of usable coherence maps (most often one or two per year), we cannot precisely extract the date of surge onset from this dataset. Therefore, we use the first sign of a frontal advance in supplementing Sentinel-1 or -2 images (if there is an advance) after a
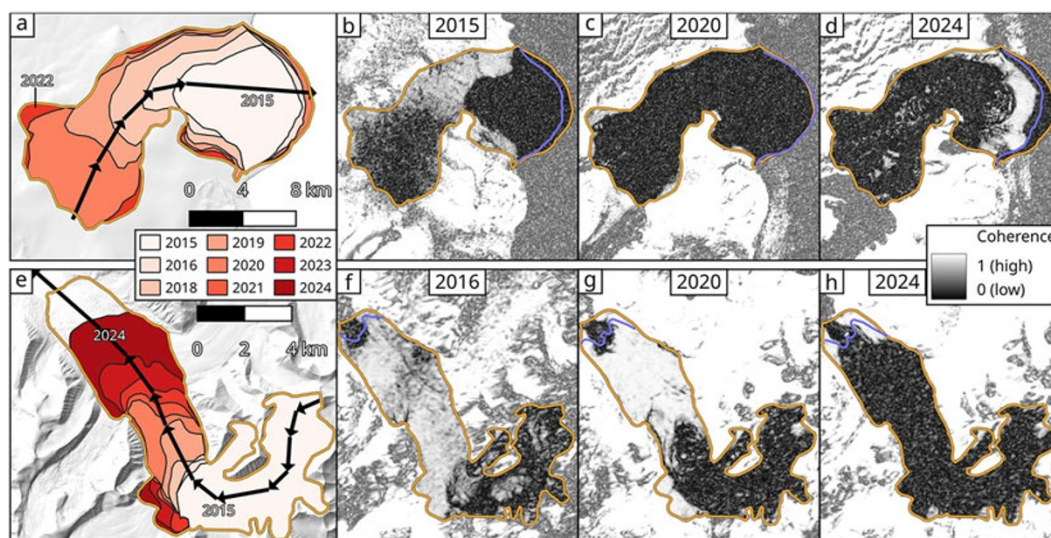
Figure 4. Examples of coherence changes during the progression of two surges. Top (a–d): terminus-initiated surge of Stonebreen. Note the onset of stagnation in 2024 (d) shown by the terminus regaining coherence. Bottom (e–h): surge bulge propagation of Paulabreen. The dates for the latter SAR acquisition in the coherence maps are (b) 21 January, (c) 3 March, (d) 22 March, (f) 29 March, (g) 1 April and (h) 23 March. The yellow outlines in all panels represent the maximum attained extent of the surges so far, and the blue lines represent the concomitant front positions. Basemap hillshade from 2010 of panels (a) and (e) courtesy of the Norwegian Polar Institute (2014). Areas outside the largest surge extents have reduced contrast to enhance visibility.
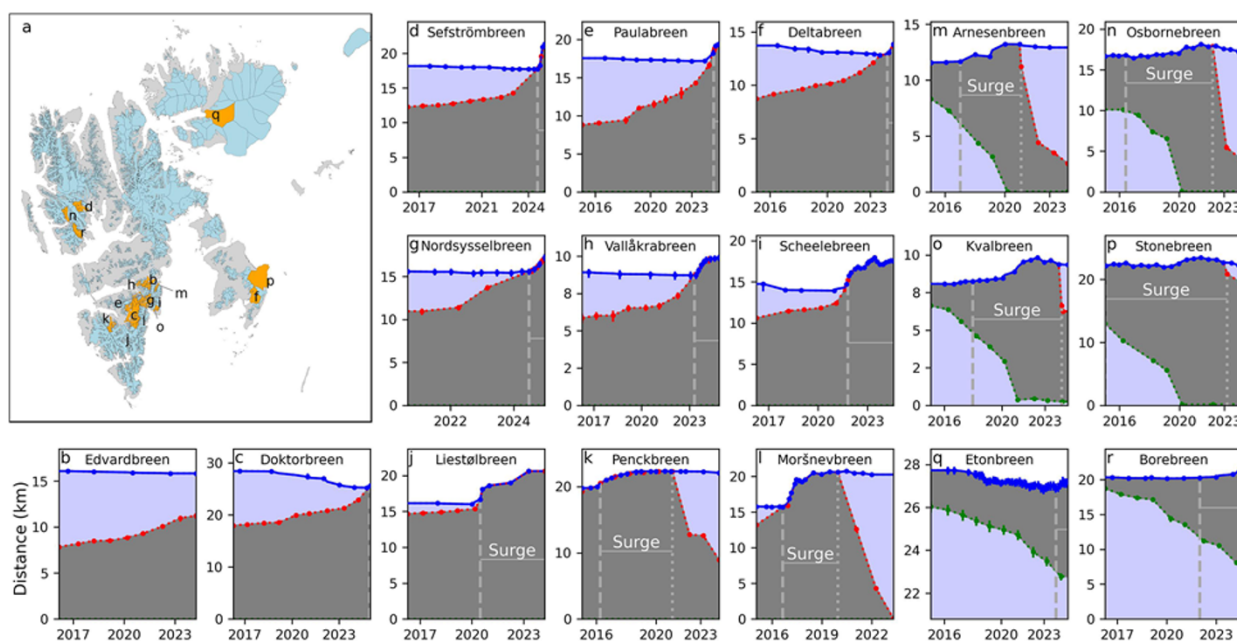

Figure 5. Digitised low-coherence (surge) front and terminus progressions for surges on Svalbard: lower low-coherence boundary/surge-front (red); terminus (blue) and upper low coherence boundary (green). See Figure 2 for the method. (a) Overview map showing all glaciers (light blue) and the location of the presented glaciers (orange plus letters). Glacier front outlines are from Nuth and others (2013). (b) Low-coherence front progression that indicates a potential future advance. (c–l) Down-glacier (bulge) propagating surge examples. (m–r) Up-glacier (terminus initiated) propagating surge examples. The y-axis represents the total distance along the centreline from the top of the glacier. High-coherence parts of the glacier are shaded light blue, low-coherence parts are shaded grey. Points (with 25th to 75th percentile spreads) represent measured values, and the parts in between are interpolated. For reference, (c) is lake-terminating, (h, i) (before reaching the sea in 2022) and (k) are land-terminating, and the rest are tidewater glaciers.

coherence map date as a more precise onset date. For up-glacier propagating surges, we choose a low-coherence expanse threshold whereafter the glacier typically starts to advance. As tidewater glaciers often naturally advance in winter due to cold waters and sea ice lowering the calving rate (Li and others, 2025), we could not use a simple advance rate threshold. We observe that all mapped up-glacier-propagated surging glaciers advanced, regardless of season, when 40% or more of the glacier had lost coherence (Fig. 3). Thus, we use this 40% coverage threshold to define the start of an up-glacier propagating surge. An exception is made at the glacier Etonbreen as it is part of an ice cap and therefore has an undefined upper bound. Instead, we used the date when the glacier first

Table 1. Statistics of the studied down-glacier (↓; bulge) and up-glacier (↑; terminus-initiated) propagating low-coherence fronts. For down-glacier propagating low-coherence fronts, the latest expected surge date ('Latest surge date' column) indicates when a linear extrapolation of the surge-front propagation from 1 year before the defined surge start would reach the glacier terminus (see Methods). The low-coherence front propagation rate follows the direction of the surge (up- or down-glacier). The terminus advance rate during the surge and the post-surge low-coherence front relaxation rate are presented. The surge advance rate is measured only within 1 year of the surge starting. Dates are reported in monthly precision to reflect the approximate precision of our measurement

Glacier	Surge kind	Surge start	Latest surge date	Surge termination	Low-coherence front propagation rate (m d^{-1})	Surge advance rate (m d^{-1})	Post-surge relaxation rate (m d^{-1})
Penckbreen	↓	Apr 2016	–	Feb 2021	6.9	4.7	8.1
Moršnevbreen	↓	Aug 2016	–	Dec 2019	4.2	9.3	12.4
Liestølbreen	↓	Jun 2020	Sep 2023	–	2.8	12.2	–
Scheelebreen	↓	Oct 2021	Apr 2030	–	6.6	9.2	–
Vallåkrabreen	↓	Apr 2023	Jul 2025	–	1.1	2.6	–
Deltabreen	↓	Mar 2024	Sep 2025	–	1.2	3.8	–
Nordsysselbreen	↓	Jun 2024	Oct 2024	–	3.0	9.4	–
Sefströmbreen	↓	Jul 2024	Dec 2028	–	1.5	16.5	–
Paulabreen	↓	Aug 2024	Feb 2026	–	5.4	20.7	–
Doktorbreen	↓	Dec 2024	Nov 2026	–	2.5	2.5	–
Edvardbreen	↓	–	Aug 2031	–	1.1	–	–
Kongsvegen	↓	–	Sep 2051	–	0.2	–	–
Stonebreen	↑	Jan 2015	–	Mar 2023	5.0	0.3	6.4
Osbornebreen	↑	Jun 2016	–	Apr 2022	5.2	0.7	17.5
Arnesenbreen	↑	Jan 2017	–	Feb 2021	5.2	0.9	13.7
Kvalbreen	↑	Dec 2017	–	Feb 2024	2.1	0.2	12.0
Borebreen	↑	Jan 2022	–	–	3.5	0.3	–
Etonbreen	↑	Nov 2023	–	–	0.8	1.3	–

advanced without the help of a sea-ice buffer (November 2023). The surge termination is defined the same for both types of surges; when the terminus regains coherence and thus shows a near or total stagnation at the front (Fig. 4). We want to highlight that the exact definition of when a surge starts and ends, where it does so and which indicators are used to define them are all up to discussion; we rather see our dates as common 'milestone' events along the continuum of surge behaviour.

Finally, we test the predictive capability of down-glacier surge progression by fitting a linear model to estimate when it will reach the front. If the surge has already started within the study period, we remove a year's worth of data from before the actual surge onset, to simulate a forecast. We fit a linear trend to three of the most recent low coherence boundary measurements (as seen in Fig. 5) and solve for the date when its length equals the most recent terminus length. We often observe an acceleration right before the surge onset and, therefore, consider this prediction a latest expected surge date rather than an exact one. We observe that the predictions indeed always occur after the true onset, ranging in differences from 4 months at best to 9 years at worst.

3. Results

As demonstration of the potential application of our method, we present statistics from 18 glaciers on Svalbard, including those with recently terminated surges, ongoing surges or those in the build-up phase. Out of these, 12 initiated after down-glacier propagation of the low-coherence zone and 6 after up-glacier propagation. We focus on aggregate statistics here; individual glacier information is found in Table 1. Unless otherwise specified, the presented numbers show the median ± standard deviation. We find that down-glacier propagating surges generally lead to significantly faster terminus advance rates (9.2 ± 6.1 m d^{-1}) compared to the up-glacier propagating counterparts (0.5 ± 0.4 m d^{-1}). However, the low-coherence front propagation generally shows an opposite tendency, with up-glacier propagation rates of 4.2 ± 1.8 m d^{-1} and down-glacier propagation rates of 2.6 ± 2.3 m d^{-1}. The latter number aligns well with the surge front propagation rates measured by

other means to 2.7–4.9 m d^{-1} at Bakaninbreen from 1985 to 1989 (Murray and others, 1998). We qualitatively note an accelerating tendency of both up- and down-glacier propagation rates near the beginning of the phase when the terminus advances (Fig. 5). There is only a weak correlation between low-coherence front propagation rates and subsequent advance rates in our data, showing Pearson correlation coefficients of 0.2 and −0.3 for down- and up-glacier propagating surges, respectively. In other words, there seems to be no simple way to predict the magnitude of a surge before it accelerates from these data alone.

The most consistent measured rate is the gradual return to coherence after a surge. Figure 4d demonstrates the ongoing stagnation of the recent Stonebreen surge, shown by regained high coherence at the terminus. All stagnating glaciers in this study show the same pattern of starting at the terminus and gradually continuing up-glacier. This occurs at a rate of 12.2 ± 4.0 m d^{-1}, with little to no variability between down- and up-glacier propagated surges.

4. Discussion

The InSAR coherence loss patterns over time that we exploit in this method test appear to have a close connection to small changes in ice dynamics that subsequently develop into surges. The promising potential of this approach is, however, complicated by the fact that most resultant coherence maps (in the maritime Svalbard climate) are dominated by widespread meteorological coherence losses over the scenes, often hiding the sought out signal of changes in ice dynamics. Where available, 6 day interferograms show much higher coherence on Svalbard than the 12 day counterparts that we use here, and the recent successful replacement of the non-functional Sentinel-1B with Sentinel-1C opens the doors for a continuation of this method using 6 day coherence instead. Despite the limitations from meteorological coherence loss and availability of certain temporal baselines, the largely uninterrupted Sentinel-1 InSAR coherence time series that we exploit represent an impressively consistent and robust data set to track surge evolution in its early phases.
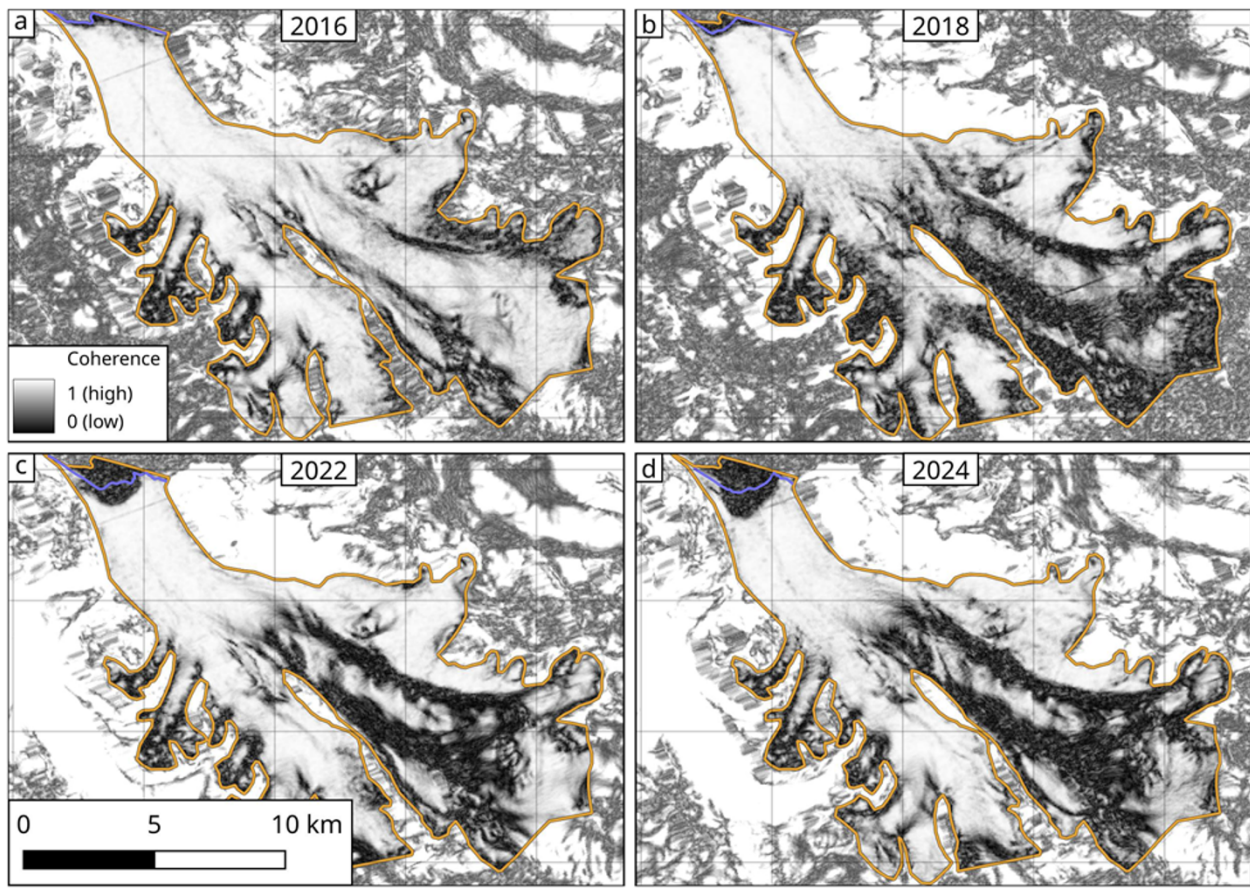
Figure 6. Early surge bulge detection at Kongsvegen, observed visually through changes in InSAR coherence maps. The 5 × 5 km grid cells show that little progression is observed, but shear margins along the bulge show a progressive reduction in coherence. The yellow outlines in all panels represent the maximum extent of the glacier throughout the study period (2016-), and the blue lines represent the concomitant front positions. The dates for the latter SAR acquisition in the coherence maps are (a) 10 April, (b) 19 March, (c) 3 April and (d) 23 March. Areas outside the largest surge extents have reduced contrast to enhance visibility.

The identified and described surges in this study display a perhaps surprising similarity in rates and patterns of propagation, advance and subsequent stagnation. Most down-glacier propagating surges have a well-defined boundary between low and high coherence, with only a few edge cases where shear margins (stripes of low coherence) are seen instead (Fig. 4). But the similarities should not instil overconfidence in the method, as we abandoned the characterisation of the recent surges of Monacobreen (Banerjee and others, 2022) and Tunabreen (Vallot and others, 2019); both glaciers are fast-flowing even during quiescence, featuring low glacier-wide coherence, and surge propagation monitoring is, therefore, not possible with our method alone. The current implementation of our method is also based on the assumption that a surge always eventually leads to an advance. This is not a necessity; the majority of High Mountain Asia surges never reach the terminus (Guillet and others, 2022), and locally confined (also termed incomplete or partial) surges have indeed been described as an occasional occurrence on Svalbard as well (Murray and others, 1998; Sund and others, 2009). While we found no clear indication of a surge that subsided before affecting the front over our 10 year study period, we acknowledge the need of an expansion of the surge classification scheme for future implementations.

An outstanding question in this work is how the initial formation of a down-glacier propagating instability looks like. In other words, how far back in time can we detect a future down-glacier propagating surge? We only have vague indications of initial bulge formation; low-coherence lines associated with shear margins gradually lose coherence and subsequently start progressing down-glacier. This is exemplified at the surge of Paulabreen in Figure 4, where the 2016 scene displays only partial loss of coherence in the surge front, while the latter scenes show a total loss. This type of proto-bulge can be seen in other examples throughout Svalbard (Fig. 6) and might represent the earliest detectable stage of unstable flow through this method. While interpretations turn vague too far back in time, we still see that many surges can be seen up to (and maybe longer than) 8 years before they reach the front. Thus, mapping the progression of low-coherence zones on glaciers can be used as an early warning system for many surges.

We do not mean to convey that all cases of lost coherence mean that a surge is about to happen. Persistent low-coherence zones that could be misclassified as surge bulges are found all over Svalbard and are most easily explained through uneven variations in subglacial topography leading to local high flow gradients and thus a reduction in coherence. In addition, all tidewater glaciers seem to feature a low-coherence zone near their termini, explainable by a steepening and acceleration leading to large deformation and crevassing near their calving bays (Murray and others, 2003a). What differentiates a potential surge from both of these cases

in the coherence is the temporal progression; an expanding disturbance or an accelerating large terminal low-coherence zone indicates a state change in the glacier's local flow characteristics. Therefore, we are confident that all our presented examples represent actual surges, but we could have missed less prominent low-coherence front propagations that represent smaller ice flow instabilities.

5. Conclusion

Here, we present InSAR coherence maps as a new tool to track glacier surge evolution from its build-up phase to stagnation. While the method is only proven to work on glaciers with low baseline quiescent velocities, the ones we study show clear similarities in surge evolution rates. There is a strong case for future automation of the tool to detect surge-like glacier flow instabilities, as the ones mapped in this study are clearly visible in the coherence data with the naked eye. We could infer glacier surges many years (in one case up to eight) before they reached the front, supporting the potential use of the method for safety-related or scientific forecasting of surge-like behaviour. We believe that the method can provide new insights into the physics and evolution of glacier surges, for instance regarding the spatio-temporal patterns of initial ice-flow change. For example, our (limited) study for Svalbard suggests that the surge front propagation (parsed from low coherence) during the build-up phase has no direct correlation with the magnitude of a later surge, meaning the physics that drive them might be different. As another potentially important result, we want to highlight that the propagation of fast flow that eventually led to surging started many years before accelerating and advancing. This has implications for studies that investigate connections between meteorological or climatic conditions and glacier surging, as a substantial time delay between build-up conditions and the subsequent surge might have to be considered. We thus suggest the use of this simple method as a complement to the existing suite of methods for detecting, mapping, classifying and tracking surges and other surge-like glacier flow instabilities.

References

Altena B, Scambos T, Fahnestock M and Kääb A (2019) Extracting recent short-term glacier velocity evolution over southern Alaska and the Yukon from a large collection of Landsat data. *The Cryosphere* **13**(3), 795–814. doi: 10.5194/tc-13-795-2019

Atwood DK, Meyer F and Arendt A (2010) Using L-band SAR coherence to delineate glacier extent. *Canadian Journal of Remote Sensing* **36**(sup1), S186–S195. doi: 10.5589/m10-014

Banerjee D, Garg V and Thakur PK (2022) Geospatial investigation on transitional (quiescence to surge initiation) phase dynamics of Monacobreen

tidewater glacier, Svalbard. *Advances in Space Research* **69**(4), 1813–1839. doi: 10.1016/j.asr.2021.08.020

Bazai NA and 7 others (2021) Increasing glacial lake outburst flood hazard in response to surge glaciers in the Karakoram. *Earth-Science Reviews* **212**, 103432. doi: 10.1016/j.earscirev.2020.103432

Bhambri R, Hewitt K, Kawishwar P and Pratap B (2017) Surge-type and surge-modified glaciers in the Karakoram. *Scientific Reports* **7**(1), 15391. doi: 10.1038/s41598-017-15473-8

Bouchayer and 7 others (2024) Multi-scale variations of subglacial hydro-mechanical conditions at Kongsvegen glacier, Svalbard. *The Cryosphere* **18**(6), 2939–2968. doi: 10.5194/tc-18-2939-2024

Clarke GK (1976) Thermal regulation of glacier surging. *Journal of Glaciology* **16**(74), 231–250. doi: 10.3189/S0022143000031567

Eldhuset K, Andersen PH, Hauge S, Isaksson E and Weydahl DJ (2003) ERS tandem InSAR processing for DEM generation, glacier motion estimation and coherence analysis on Svalbard. *International Journal of Remote Sensing* **24**(7), 1415–1437. doi: 10.1080/01431160210153039

Farnsworth WR, Ingólfsson O, Retelle M and Schomacker A (2016) Over 400 previously undocumented Svalbard surge-type glaciers identified. *Geomorphology* **264**, 52–60. doi: 10.1016/j.geomorph.2016.03.025

Frey H, Paul F and Strozzi T (2012) Compilation of a glacier inventory for the western Himalayas from satellite data: Methods, challenges, and results. *Remote Sensing of Environment* **124**, 832–843. doi: 10.1016/j.rse.2012.06.020

Guillet G and 6 others (2022) A regionally resolved inventory of High Mountain Asia surge-type glaciers, derived from a multi-factor remote sensing approach. *The Cryosphere* **16**(2), 603–623. doi: 10.5194/tc-16-603-2022

Harcourt WD and 8 others (2025) *Surging Glaciers in Svalbard: Current Knowledge and Perspectives for Monitoring SvalSurge*. Technical report. Longyearbyen, Norway: Svalbard Integrated Arctic Earth Observing System. doi: 10.5281/ZENODO.14425522

Herreid S and Truffer M (2016) Automated detection of unstable glacier flow and a spectrum of speedup behavior in the Alaska Range. *Journal of Geophysical Research: Earth Surface* **121**(4), 64–81. doi: 10.1002/2015JF003502

Hugonnet R and 6 others (2022) Uncertainty analysis of digital elevation models by spatial inference from stable terrain. *IEEE Journal of Selected Topics in Applied Earth Observations and Remote Sensing*, 1–17. doi: 10.1109/JSTARS.2022.3188922

Kääb A, Bazilova V, Leclercq PW, Mannerfelt ES and Strozzi T (2023) Global clustering of recent glacier surges from radar backscatter data, 2017–2022. *Journal of Glaciology* **69**(277), 1515–1523. doi: 10.1017/jog.2023.35

Koch M, Seehaus T, Friedl P and Braun M (2023) Automated detection of glacier surges from Sentinel-1 surface velocity time series – An example from Svalbard. *Remote Sensing* **15**, 1545. doi: 10.3390/rs15061545

Li T and 6 others (2025) Pervasive glacier retreats across Svalbard from 1985 to 2023. *Nature Communications* **16**(1), 705. doi: 10.1038/s41467-025-55948-1

Murray T, Dowdeswell JA, Drewry DJ and Frearson I (1998) Geometric evolution and ice dynamics during a surge of Bakaninbreen, Svalbard. *Journal of Glaciology* **44**, 263–272. doi: 10.3189/S0022143000002604

Murray T, Luckman A, Strozzi T and Nuttall AM (2003a) The initiation of glacier surging at Fridtjovbreen, Svalbard. *Annals of Glaciology* **36**, 110–116. doi: 10.3189/172756403781816275

Murray T, Strozzi T, Luckman A, Jiskoot H and Christakos P (2003b) Is there a single surge mechanism? Contrasts in dynamics between glacier surges in Svalbard and other regions. *Journal of Geophysical Research: Solid Earth* **108**(B5), 2237. doi: 10.1029/2002JB001906

Norwegian Polar Institute (2014) *Terrengmodell Svalbard (S0 Terrengmodell)*, Tromsø, Norway. doi: 10.21334/npolar.2014.dce53a47

Nuth C and 7 others (2013) Decadal changes from a multi-temporal glacier inventory of Svalbard. *The Cryosphere* **7**(5), 1603–1621. doi: 10.5194/tc-7-1603-2013

Nuttall AM, Hagen JO and Dowdeswell J (1997) Quiescent-phase changes in velocity and geometry of Finsterwalderbreen, a surge-type glacier in Svalbard. *Annals of Glaciology* **24**, 249–254. doi: 10.3189/S0260305500012258

Paul F and 9 others (2022) Three different glacier surges at a spot: What satellites observe and what not. *The Cryosphere* **16**(6), 2505–2526. doi: 10.5194/tc-16-2505-2022

Post A and LR Mayo (1971) Glacier dammed lakes and outburst floods in Alaska. *USGS Numbered Series 455*. U.S. Geological Survey: Alaska, USA. doi: 10.3133/ha455

Pritchard H, Murray T, Strozzi T, Barr S and Luckman A (2003) Surge-related topographic change of the glacier Sortebræ, East Greenland, derived from synthetic aperture radar interferometry. *Journal of Glaciology* **49**(166), 381–390. doi: 10.3189/172756503781830593

Rouyet L and 7 others (2021) Environmental controls of InSAR-based periglacial ground dynamics in a sub-arctic landscape. *Journal of Geophysical Research: Earth Surface* **126**(7), e2021JF006175. doi: 10.1029/2021JF006175

Sevestre H and Benn DI (2015) Climatic and geometric controls on the global distribution of surge-type glaciers: Implications for a unifying model of surging. *Journal of Glaciology* **61**(288), 646–662. doi: 10.3189/2015JoG14J136

Sevestre H and 6 others (2018) Tidewater glacier surges initiated at the terminus. *Journal of Geophysical Research: Earth Surface* **123**(5), 1035–1051. doi: 10.1029/2017JF004358

Shi Y, Liu G, Wang X, Liu Q, Zhang R and Jia H (2019) Assessing the glacier boundaries in the Qinghai-Tibetan Plateau of China by multi-temporal coherence estimation with Sentinel-1A InSAR. *Remote Sensing* **11**(4), 392. doi: 10.3390/rs11040392

Strozzi T, Luckman A, Murray T, Wegmuller U and Werner C (2002) Glacier motion estimation using SAR offset-tracking procedures. *IEEE Transactions on Geoscience and Remote Sensing* **40**(11), 2384–2391. doi: 10.1109/TGRS.2002.805079

Sund M and Eiken T (2004) Quiescent-phase dynamics and surge history of a polythermal glacier: Hessbreen, Svalbard. *Journal of Glaciology* **50**(171), 547–555. doi: 10.3189/172756504781829666

Sund M, Eiken T, Hagen JO and Kääb A (2009) Svalbard surge dynamics derived from geometric changes. *Annals of Glaciology* **50**(52), 50–60. doi: 10.3189/172756409789624265

Sund M, Lauknes TR and Eiken T (2014) Surge dynamics in the Nathorstbreen glacier system, Svalbard. *The Cryosphere* **8**(2), 623–638. doi: 10.5194/tc-8-623-2014

Thomas DJ, Robson BA and Racoviteanu A (2023) An integrated deep learning and object-based image analysis approach for mapping debris-covered glaciers. *Frontiers in Remote Sensing* **4**, 1161530. doi: 10.3389/frsen.2023.1161530

Vallot D and 6 others (2019) Automatic detection of calving events from time-lapse imagery at Tunabreen, Svalbard. *Geoscientific Instrumentation, Methods and Data Systems* **8**(1), 113–127. doi: 10.5194/gi-8-113-2019

Weydahl D (2001) Analysis of ERS tandem SAR coherence from glaciers, valleys, and fjord ice on Svalbard. *IEEE Transactions on Geoscience and Remote Sensing* **39**(9), 2029–2039. doi: 10.1109/36.951093